A&A 464, 1155–1166 (2007)
DOI: 10.1051/0004-6361:20065882

Astronomy & Astrophysics

The XMM-Newton EPIC background and the production of background blank sky event files⋆

J. A. Carter and A. M. Read

Department of Physics and Astronomy, University of Leicester, Leicester, LE1 1RH, UK
e-mail: [jac48;amr30]@star.le.ac.uk

Received 22 June 2006 / Accepted 22 December 2006

ABSTRACT

Aims. We describe in detail the nature of XMM-Newton EPIC background and its various complex components, summarising the new findings of the XMM-Newton EPIC background working group, and provide XMM-Newton background blank sky event files for use in the data analysis of diffuse and extended sources.
Methods. Blank sky event file data sets are produced from the stacking of data, taken from 189 observations resulting from the Second XMM-Newton Serendipitous Source Catalogue (2XMMp) reprocessing. The data underwent several filtering steps, using a revised and improved method over previous work, which we describe in detail.
Results. We investigate several properties of the final blank sky data sets. The user is directed to the location of the final data sets. There is a final data set for each EPIC instrument-filter-mode combination.

Key words. methods: data analysis – X-rays: diffuse background – X-rays: general – instrumentation: detectors

1. Introduction

The XMM-Newton observatory (Jansen et al. 2001), with the two EPIC MOS (Turner et al. 2001) and one EPIC PN (Strüder et al. 2001) cameras at the foci of the three telescopes, provides unrivalled capabilities for detecting low surface brightness emission features from extended and diffuse galactic and extragalactic sources, by virtue of the large field of view of the X-ray telescopes and the high throughput yielded by the heavily nested telescope mirrors. In order to exploit the excellent EPIC data from extended objects, the EPIC background (BG), now known to be higher than estimated pre-launch, needs to be understood thoroughly.

In 2005 a working group was set up to organise various investigations into the BG, to define the BG material useful for the general user and to place this BG material and findings of the group on the main XMM-Newton SOC web pages. This paper concentrates on one aspect of this work, namely that of the production of blank sky background event files, constructed for each of the EPIC instruments in each filter/mode combination.

The work described in this paper follows on from that of Read & Ponman (2003). The number of observations used in this analysis has increased from 72 to 189, greatly improving the signal-to-noise ratio. Further changes to the previous dataset have been the inclusion of thick filter observations in the analysis and other improvements described later.

All the background product files (event files, exposure maps, related software), together with other scripts and procedures for XMM-Newton background analysis are available from the official ESA site: `http://xmm.esac.esa.int/external/xmm_sw_cal/background/index.shtml`.

The activities of the BG working group has led to a greater understanding of the complex components that make up the XMM-Newton EPIC BG. In Sect. 2 of this paper we describe these various components, presenting a review of our current understanding of the BG. In Sect. 3 we describe the production of the blank sky event files, detailing improvements made over previous work in the filtering stages using current knowledge of the BG. In Sect. 4 we detail some properties of these files, and in Sect. 5 we discuss the use of these files and present software that we have written and made available for use with the blank sky event files. Finally, in Sect. 6 we present our conclusions and discuss future plans for analysing the BG.

2. The XMM-Newton EPIC X-ray background

Given the complex nature of the EPIC background, and that new components of the background have recently been discovered by the BG working group and others, it is appropriate that a comprehensive description of the EPIC background should be given:

The EPIC background can be separated into particle, photon and electronic noise components (as described in the work of Lumb et al. 2002; Read & Ponman 2003, and references therein). Several contributions are focused by the mirrors, whereas others arrive at the detectors directly through the shielding. The particle background can be further sub-divided into contributions from soft protons and cosmic-ray induced events, and the photon background can be sub-divided into contributions from hard and soft X-rays. In this section we describe each of these components, discussing their temporal, spectral and spatial properties. A table summarising the components of the background can be found via the official XMM-Newton pages.

⋆ Based on observations with XMM-*Newton*, an ESA Science Mission with instruments and contributions directly funded by ESA Member States and the USA (NASA).

2.1. Particle background

The particle background consists of focused soft protons and unfocused cosmic ray induced events.

2.1.1. Soft protons

This contribution to the background comes from solar soft protons, accelerated by magneto-spheric reconnection events and trapped by the Earth's magnetosphere, which are then gathered by XMM-Newton's grazing mirrors. They dominate times of high background. These soft protons occur in flares up to 1000% of the quiescent level in an observation. They are highly unpredictable and affect 30% to 40% of XMM-Newton observation time. The frequency of soft protons seen increases closer to perigee. Within a single observation, a significant component may survive after good time interval screening (de Luca & Molendi 2004). Spectrally the soft protons are variable in intensity and shape. For energies >0.5 keV the continuum spectrum, which shows no lines, can be fitted by an unfolded Xspec power law, i.e. one not convolved with the instrumental response (specifically a double-exponential or broken power law, with the break energy at approximately 3.2 keV, and with the spectrum becoming flatter at higher intensities). Below 0.5 keV, much less flux is seen (Kuntz et al. in preparation). The soft protons are distributed over the detector in a similar manner to X-rays, but the vignetting function is flatter than for photons. Also for the low-energy soft protons the vignetting function is flatter than that of high-energy protons. They are only observed inside the FOV (though during times of intense solar flares (which are unfocused), the out-FOV signal can be greatly increased). There is no other spatial structure seen in the PN, but some structure may occur in the MOS due to the presence of the Reflection Grating Array on board XMM-Newton. An as yet poorly understood soft proton feature is seen in MOS CCD-2 at low energies (Kuntz et al., in prep.).

2.1.2. Internal cosmic ray induced events: the instrumental BG

This component of the BG results from high-energy particles producing charge directly in the CCDs, and from the interaction of high energy particles with the detector, causing associated instrumental fluorescence. Within an observation this component can vary by up to 10%. For the MOS cameras above 2 keV there is no change seen in the continuum and only small changes seen in the fluorescence lines, but below 1.5 keV the continuum varies, possibly due to the redistribution of the Al calibration line (de Luca & Molendi 2004). From observation to observation there is some variation; up to 10 times more intense an effect can be seen during periods of intense solar flares, but no increase is seen after the occurrence of solar flares so activation is unlikely.

The continuum spectrum is flat (with an index ∼0.2). The instrumental fluorescence lines for MOS are found at 1.5 keV (Al-K), 1.7 keV (Si-K), plus some contribution from high energy lines (Cr, Mn, Fe-K and Au). For the PN, Al-K is seen at 1.5 keV, whereas the silicon line is self-absorbed, and high energy contributions are seen from Cu, Ni, Zn and K. Detector noise occurs below 0.3 keV.

The internal instrumental BG has a spatial distribution different from that of X-ray photons as it is not vignetted. In the outer CCDs and outside the field of view (FOV) for MOS there is more Al seen than Si, whereas the CCD edges show enhanced Si. There are continuum differences between the out-FOV and in-FOV below the Al-line, possibly resulting from redistribution. There is more Au seen out-FOV due to the Al-shielding which is coated with gold on its inner surfaces. Energies and widths of the lines are stable, whereas line intensities can vary. In the PN, line intensities show large spatial variation from the electronics board, for example the well-known "copper hole", where a deficit in high-energy instrumental lines is seen at the detector centre (Freyberg et al. 2004). Residual low-energy instrumental BG components are seen near the CAMEX readout areas.

2.2. Electronic noise

Electronic noise results from bright pixels and parts of columns, CAMEX readout noise in the PN and artificial low-energy enhancements in the outer CCDs of MOS. Dark current may also contribute, but this is thought negligible.

No temporal variations are seen within an observation apart from the bright pixel and column component that can vary by up to 10%. Bright pixels fluctuate greatly between observations. For the PN, the CAMEX readout noise is mode dependent; extended-full-frame mode suffering the least from this noise, and small window mode the most. Artificial low-energy enhancements may affect up to 20% or more of observations, and are enhanced during periods of high BG rate.

Spectrally, this component is seen at low energies (below 300 eV) for the bright pixel and CAMEX readout contributions. Artificial low-energy enhancements are sometimes observed below 500 eV in certain MOS CCDs (Kuntz et al., in prep.; Pradas & Kerp 2005).

This component is distributed differently from genuine X-ray photons and is not vignetted, apart from the artificial low-energy enhancements in the MOS cameras. The bright pixels and columns are seen at certain locations; structure is seen near to the PN readout (CAMEX). Certain MOS CCDs show some peculiarities in and out of FOV (Kuntz in prep.) and spatial inhomogeneities are seen within a particular MOS CCD.

2.3. Photon background

The photon background can be split into components from hard and soft X-rays and these components are focused by the mirrors.

2.3.1. Hard X-ray photons

The hard X-ray background photons mainly originate from unresolved AGN within the FOV. There are also single reflections into the FOV from all kinds of out-FOV sources, both bright and faint, resolved and unresolved (the unresolved out-FOV sources being, as for the in-FOV, predominatly AGN). Out-of-time events (OOT) are also a contributor to the hard X-ray BG of the PN.

The hard X-ray photon BG does not vary within an observation or between observations, although OOT events are mode dependent for the PN; the full-frame mode experiencing more of this effect than both the extended-full-frame and large window mode, due to the percentage of the frame time used for readout.

The hard X-ray photon BG can be modelled by a power law of spectral index ∼1.4. In times of low-BG, and below 5 keV, this component dominates over the internal component of the BG, whereas above 5 keV, the internal component dominates. As they are genuine X-ray photons, they are spatially vignetted.

Diffuse flux from single reflections gathered from out-of-field angles of 0.4−1.4 degrees that are reflected into the FOV ("single reflections"), contribute ∼7% of the in-FOV flux (Lumb et al. 2002), and the effective area of one of the telescopes is approximately 3 cm^2 at 20−80′ off-axis (Freyberg et al. 2004). OOT events are smeared along the readout direction from the bright X-ray sources of X-rays (Freyberg et al. 2004).

2.3.2. Soft X-ray photons

Soft X-rays originate from the Local Bubble, Galactic Disk, Galactic Halo, the Solar Wind Charge Exchange (SWCX) (Snowden et al. 2004) single reflections from outside the FOV and OOT events (PN only). The SWCX is an interaction between the highly ionised solar wind and either interstellar neutrals in the heliosphere or materials in the Earth's exosphere. There is little variation seen in the soft X-ray BG during a single observation, although long observations may be affected by the SWCX. Variations of up to 35% are seen between observations as observation pointings differ in Right Ascension and Declination. Also, the SWCX component may effect observations differently.

The diffuse contributions from the Local Bubble, Galactic Disk and Galactic Halo have a thermal component with emission lines ∼<1 keV. The extragalactic component above 0.8 keV has an index of 1.4, whereas the galactic contribution in terms of emission and absorption varies. The SWCX component is very soft and comprises unusual OVIII/OVII line ratios and strong OVIII and MgXI features.

The soft X-ray BG component is vignetted as it is made up of genuine X-ray photons. Spatially, the only structure seen is from real astronomical objects, and the extragalactic component above 0.8 keV is spatially uniform. The SWCX is seen over the whole FOV. The single reflections and OOT events behave as those resulting from hard X-rays.

The BG has shown itself to be extremely complicated and made up of various different components. When performing detailed XMM-Newton EPIC analysis, a good knowledge of the background is required. Sometimes it may be possible to extract the background from a region close to the particular source one is interested in (using a so-called "local" background). For a large or extended source however, one may have to extract the background far from the target source (the source may in fact be so extended, that no local background is visible within the field of view). Here, a number of effects, due to many of the features described above, can cause the extracted local (off-axis) background to be highly inappropriate in analysing the (normally on-axis located) target source, such as changes in the effective area of the mirrors with off-axis angle, instrumental fluorescence and the spectral response which can depend on the position on the detector (these off-axis effects are corrected in the XMM-Newton EPIC calibration). Hence the need for blank sky background event files for the general user to study diffuse and extended sources, where images from XMM-Newton do not provide suitable selection areas for background subtraction.

3. Blank sky analysis

The data processing described here has resulted in the production of new XMM-Newton background event files for the 3 EPIC instruments in their different instrument mode/filter combinations. These have been constructed using a superposition of many pointed observations of pipeline product data from the Second XMM-Newton Serendipitous Source Catalogue (2XMMp) reprocessing: (`http://xmm.esa.int/external/xmm_user_support/documentation/uhb/`) and have been processed with version of the SAS 6.5.0.

These files are available at the website location as mentioned in the introduction.

In the case of PN, in full-frame mode, for the medium and thin filter, it was necessary to split the event files, as the size of these files exceeded that of the maximum that is usable with FTOOLS and the XMM-Newton Science Analysis System (SAS). This is explained in more detail below.

In total 189 observations were analysed from the 2XMMp reprocessing. The observations were selected based on the absence of a large diffuse component or significantly bright source whose wings could still contaminate the background after source subtraction. Observations with bright central sources were avoided. Therefore observations of fields such as the Lockman Hole, Hubble Deep Field North and Marano pointings etc. were of particular use, and the archive was scanned for useful survey fields. All available observations that were used by previous background studies (Read & Ponman 2003; Nevalainen et al. 2005; Lumb et al. 2002) were included.

Table 1 lists the observations used in this analysis.

The final event lists result from the stacking of pipeline product event lists from many observations that have been subjected to various filtering steps, which includes the removal of sources (as described below). Therefore proper consideration of the exposure maps is required when using the final event list that applies to a set of combined observations.

Each observation was subjected to the same initial analysis. The steps in this procedure were as follows:

- the relevant 2XMMp pipeline processing system products (PPS) (event lists, attitude files, background time series, source files and calibration index files) are collected together;
- for each instrument, region files are created from the PPS source lists. These are then used to remove all the source events from each of the relevant event files. A conservative extraction radius of 35″ is used to remove the sources (for comparison, Read & Ponman 2003, used 36″; and Lumb et al. 2002, used 25″). These regions are also removed from previously created mask files (these are required to calculate losses in area due to source removal);
- a visual inspection is made of the data to make sure that there are no strange features in the field (such as the rings seen from off-axis single reflections), and to ascertain whether there are any wings of very bright point sources or large diffuse sources which could contaminate the background, even after source subtraction. Datasets which fail this inspection are rejected from any subsequent analysis;
- the event files are then filtered further. Events with energies below 100 eV are discarded. For PN, only singles and doubles are retained, for MOS 1 and MOS 2, singles, doubles, triples and quadruples are retained. Finally, the event lists are filtered using the SAS-recommended *#XMMEA_EM* and *#XMMEA_EP* FLAG expressions, excepting that events from outside the field of view (out-FOV) are also kept;
- each of the event files are then conservatively filtered for periods of high background (solar proton flares) by first creating Good Time Interval (GTI) files from the pipeline processing products background time series files and then applying these GTI files to the event file. Upper count rate threshold of 60 (PN) and 2 (MOS1/MOS2) ct/s are used as

Table 1. Summary of all the observations used. IMF gives the instrument, mode and filter for PN-MOS1-MOS2 as [f = full-frame, e = full-frame-extended, t = thin, m=medium, k = thick and NA - not applicable]. Exp. is the cleaned exposure time, and f(Ex) the fraction of exposure removed after screening (where possible PN or alternatively MOS1).

Obs	IMF	Exp. (s)	f(Ex)	Obs.	IMF	Exp.	f(Ex)	Obs.	IMF	Exp. (s)	f(Ex)
0123700101	ftftfk	46561	0.192	0125300101	ftftft	38127	0.002	0126511201	fkfkfk	29205	0.018
0110980401	etftft	39999	0.015	0112940201	etftft	5898	0.002	0112940301	etftft	6099	0.000
0112940401	etftft	5898	0.000	0112940501	NAftft	7184	0.254	0127921001	etftft	51496	0.000
0127921201	etftft	14699	0.000	0112370101	NAftft	57523	0.168	0112371001	ftftft	56766	0.075
0102640201	emfmfm	13300	0.000	0112370301	NAftft	63066	0.204	0112371501	ftftft	8300	0.019
0112371701	ftftft	25247	0.002	0129320801	emfmfm	6199	0.000	0129320901	etftft	6197	0.000
0129321001	NAftft	5039	0.000	0112230901	etftft	23948	0.307	0112231001	etftft	24485	0.004
0112970701	emfmfm	19519	0.000	0094800201	etftft	48056	0.306	0110660301	etftft	4855	0.110
0104460301	fmfmfm	9649	0.000	0128530301	NAftft	37446	0.153	0113891201	fmfmfm	19456	0.052
0106660101	ftftft	54807	0.000	0099030101	ftNANA	19946	0.048	0110660401	emfmfm	9287	0.015
0110980101	etftft	50256	0.046	0112650401	etftfm	19999	0.000	0134531201	fkfkfk	18999	0.000
0134531301	fkfkfk	6024	0.000	0007420701	fmfmfm	9700	0.000	0007420801	fmfmfm	12305	0.000
0007421001	fmfmfm	9514	0.048	0007421901	fmfmfm	7999	0.000	0007422001	fmfmfm	7599	0.000
0007422101	fmfmfm	9400	0.000	0007422201	fmfmfm	9400	0.000	0007422301	fmfmfm	12650	0.000
0093640901	emfmfm	5899	0.007	0111120201	fmfmfm	30377	0.000	0022140101	emfmfm	11156	0.000
0093670501	emfmfm	9155	0.000	0021750701	fkfkfk	25649	0.000	0024140101	fkfkfk	58270	0.000
0067340201	emfmfm	9949	0.000	0135740901	fmfmfm	9250	0.000	0081341001	ftftft	19602	0.060
0006010301	fkfkfk	31929	0.000	0070340301	emfmfm	26429	0.473	0111550101	ftftft	42381	0.013
0111550201	ftftft	41095	0.012	0092970201	emfmfm	8980	0.000	0093640701	emfmfm	15065	0.000
0111550401	ftftft	91805	0.005	0134531401	fkfkfk	11842	0.709	0032140201	fmfmfm	9839	0.135
0109660801	ftftfm	62945	0.076	0051760201	ftftft	18260	0.047	0109660901	ftfmft	42812	0.341
0109661001	ftftft	80575	0.077	0110990201	etftft	24614	0.189	0109520501	etftft	19960	0.000
0111110301	etftft	20010	0.000	0111110401	etftft	22421	0.000	0111110501	etftft	20039	0.000
0111110101	etftft	20898	0.009	0111110201	etftft	8196	0.263	0111280301	etftft	4960	0.119
0112250301	etftft	21955	0.000	0137750101	ftftft	16360	0.000	0057560301	ftftft	37681	0.015
0112220101	fmfmfm	37390	0.000	0093630101	fmfmfm	13199	0.000	0111110701	etftft	8399	0.000
0000110101	fmfmfm	28811	0.100	0067750101	ftftft	44219	0.180	0016140101	NAfmfm	32945	0.459
0112190401	emfmfm	9994	0.002	0112410101	ftftft	9609	0.006	0112460201	fmfmfm	36447	0.135
0002740101	ftftft	29685	0.102	0089940201	ftftft	30082	0.074	0111160201	etftft	44373	0.001
0112480101	etftft	15664	0.000	0112480201	etftfm	13288	0.000	0094400101	fmfmfm	29283	0.000
0050940301	emfmfm	9098	0.035	0137950201	ftftft	21529	0.070	0137950301	ftftft	22500	0.000
0050150301	ftftft	25133	0.060	0109260201	ekfkfk	28453	0.000	0032140501	fmfmfm	9971	0.000
0092360201	etftft	9935	0.000	0079570201	emfmfm	43075	0.092	0094400301	fmfmfm	19978	0.000
0021740101	emfmfm	29888	0.021	0022740201	fmfmfm	61189	0.012	0094530401	etftft	19923	0.000
0092360101	etftft	7399	0.000	0092360301	etftft	9872	0.110	0092360401	etftft	8599	0.000
0092800101	fmfmfm	14277	0.000	0134531501	fkfkfk	18484	0.000	0109463501	ftftft	5000	0.000
0028740301	ftftft	25863	0.000	0046940401	emfmfm	10598	0.000	0083240201	etftft	15699	0.001
0086750101	ftftft	8595	0.123	0022740301	fmfmfm	36366	0.009	0085170101	ftftft	29937	0.000
0085640201	etfmfm	29904	0.000	0049340201	fmfmfm	24558	0.000	0112190601	emfmfm	10540	0.000
0106660401	NAftft	34391	0.025	0106660501	ftftft	8076	0.169	0070940101	NAftft	9924	0.411
0026340201	emfmfm	13906	0.237	0112551201	emftft	9999	0.000	0055990301	etftft	9999	0.000
0033541001	ftftft	9912	0.000	0052140201	emfmfm	36228	0.036	0059800101	etftft	5769	0.000
0112550501	emftft	18499	0.000	0011830201	ftftft	32653	0.065	0002970401	NANAft	3640	0.001
0112810201	ftftft	13000	0.085	0033540901	ftftft	14444	0.027	0037980101	etftft	10177	0.000
0037980201	etftft	8999	0.000	0037980301	etftft	9099	0.000	0037980601	etftft	8992	0.000
0037980701	etftft	7999	0.000	0037980401	etftft	10378	0.071	0037980501	etftft	12951	0.022
0037980901	etftft	9999	0.000	0109520601	etftft	18981	0.000	0109520301	etftft	17961	0.000
0112680401	ftftft	21991	0.000	0109110101	emfmfm	71843	0.000	0025740401	ftftft	17449	0.146
0083950101	emfmfm	23222	0.026	0081341101	ftftft	17105	0.000	0109280101	ekfkfk	19796	0.000
0112480301	etftft	13533	0.000	0050940101	emfmfm	19999	0.048	0006010401	fkfkfk	32932	0.000
0026340101	etftft	21932	0.000	0058940101	emfmfm	23793	0.000	0110661601	etftft	5999	0.000
0051610101	emfmfm	17960	0.000	0026340301	emfmfm	19829	0.008	0092800201	fmfmfm	92855	0.095
0082140301	emfmfm	28892	0.000	0112190201	emfmfm	9999	0.000	0111280601	etftft	7176	0.000
0111282001	etftft	4999	0.003	0103060301	etftft	42728	0.034	0111280701	etftft	4992	0.005
0111280801	etftft	4999	0.000	0111282201	etftft	4999	0.000	0037980801	etftft	9999	0.011
0112551501	ekftft	17749	0.000	0037981001	etftft	9999	0.000	0037981101	etftft	9867	0.000
0037981201	etftft	9753	0.045	0110662701	emfmfm	6291	0.383	0147510101	fmfmfm	90984	0.020
0147510801	fmfmfm	75660	0.047	0147510901	fmfmfm	88534	0.066	0147511101	fmfmfm	93394	0.216
0147511201	fmfmfm	100499	0.363	0147511301	fmfmfm	82459	0.182	0145450401	ftftft	5748	0.000
0145450501	ftftft	5847	0.004	0147511601	fmfmfm	121142	0.038	0147511801	fmfmfm	88811	0.000
0112372001	ftftft	25950	0.000	0037982401	etftft	11605	0.000	0037982501	etftft	10415	0.000
0037982301	etftft	9999	0.008	0037982201	etftft	12699	0.001	0140160101	fkfkfk	41606	0.068
0145450101	ftftft	8152	0.147	0145450601	ftftft	7978	0.038	0149890301	ftftft	39996	0.318

recommended as conservative thresholds by the EPIC instrument teams;
- in the case of PN, it was necessary to further filter the files to clean a small number of persistent bad (bright) pixels/columns, occurring in many (though not all) of the observations. Events were removed from all PN datasets below 250 eV, as follows: CCD1 Col. 13 and pixels RAWX, Y = (56,75), CCD2 RAWX, Y = (46−47,69−72), CCD5 Col. 11 and RAWX, Y = (41, 182−184), CCD7 Col. 34, CCD10 Col. 61, CCD11 RAWX, Y = (47−48,153−156) and RAWX, Y = (50,161−164). No bad pixels were removed from any of the MOS datasets. The event files are now filtered and have had all sources removed;
- ghosting of events, if applicable, is applied by an IDL code (see Sect. 3.1). The use of this procedure results in *refilled* event list, after the completion of the tasks below. Therefore there are two types of final files: *refilled* files that have gone through the ghosting procedure, and *unfilled* files that have not;
- for each of the three instruments, a non-vignetted and vignetted 4″ exposure map is created. For the unfilled sets, the procedure was more complex than that of the filled sets, as the sources removed had to be taken into account. From the source-removed mask file, an area map (4″ binning) is created, containing zero values at the positions where sources have been removed, and unity values elsewhere. This is combined with the 4″ exposure map to create a source removed exposure map;
- to each event, values of Right Ascension and Declination are given in newly formed columns, using the information from the original event file header *RA_PNT* and *DEC_PNT* keywords.

3.1. Ghosting of events

There are two types of background event lists; unfilled and refilled. In the case of the refilled event lists, a method has been developed to "fill in" the source regions that are extracted from each individual observation by sampling events close to the extracted regions, copying these events and filling the vacated region of the event list, randomising just the spatial (*DETX, DETY*) coordinates. Great care was taken when making adjustments for region crossovers, instrument boundaries and chips edges. This results in smooth event file images and exposure maps. Both types of event file are available at the aforementioned website, with corresponding vignetted and non-vignetted exposure maps. As the ghosted events in this code are based on *DETX, DETY* coordinates, it is necessary to use the SAS task *attcalc*, setting right ascension, declination and pointing angle to (0, 0, 0) to re-project these events in terms of X and Y. Figure 1 shows an example individual observation prior to and post the ghosting procedure. Figure 2 shows an image created from one of the final PN files made up of event files that have been subjected to the ghosting procedure, between 7.8 keV and 8.2 keV, which illustrates that the ghosting procedure slightly blurs the edges of the "copper hole" as described in Sect. 2.1.2, but is still of minimal significance. It is hoped in the future that we will be able to develop the ghosting procedure to ghost bad columns and pixels (see Sect. 6).

3.2. Properties of the observations used

Some features of the data sets used for MOS1 can be seen in Fig. 3. The equivalent figures for MOS2 and PN look essentially identical. Figure 3a shows a histogram of the livetime values for MOS1 after cleaning. The average values of livetimes after cleaning were 21 647 s for MOS1, 21 682 s for MOS2 and 20 357 s for PN, hence the files are very representative of the XMM-Newton average exposure of ∼22 950 s (based on ∼11 200+ EPIC exposures). Observations were taken for all instruments from between revolution 70 and 691, and hence cover a good fraction of the mission. The distribution of revolution numbers for MOS1, is shown in Fig. 3b. This figure also plots a histogram of the fraction of time removed per observation, and also the fraction of time removed per month, for MOS1 (3c and d). The average fraction of time removed for MOS1 was 0.8098, 0.8190 for MOS2 and 0.9577 for PN, which reflects the conservative cutting levels used in the cleaning. There is no evidence that the month of the observation affects the fraction of time removed from the observation. Figure 3c shows a histogram of the column density values towards each MOS1 pointing. The column density values have a peak at $\sim 2.5 \times 10^{20}$ cm^{-2}, which is very typical for an average XMM-Newton pointing. Figure 3f shows the total livetimes after cleaning for MOS1 per month. There is a fairly even distribution of observations throughout the year.

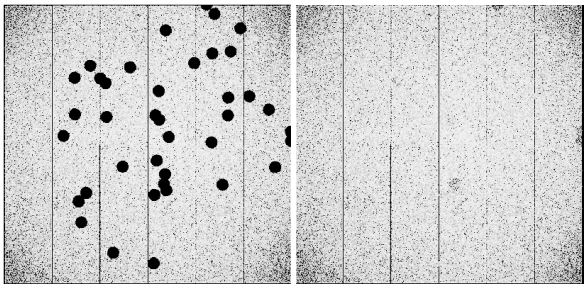

Fig. 1. Images from a PN observation with the source holes removed prior to the ghosting procedure (*left*) and after the ghosting procedure (*right*). Although there are slight problems in the ghosting procedure in very source confused areas, no problems remain after stacking of several such filled event files.

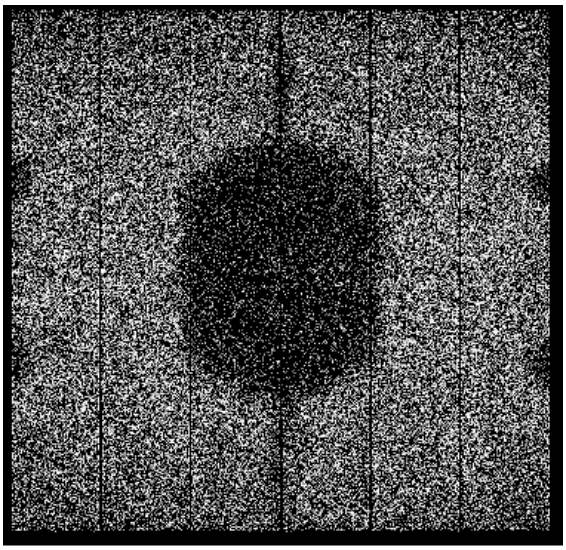

Fig. 2. An image created from one of the final refilled event files for PN, thin filter, full-frame mode, between the energies of 7.8 keV and 8.2 keV. This shows the copper hole and the slight blurring of the edges of this feature due to the ghosting procedure.

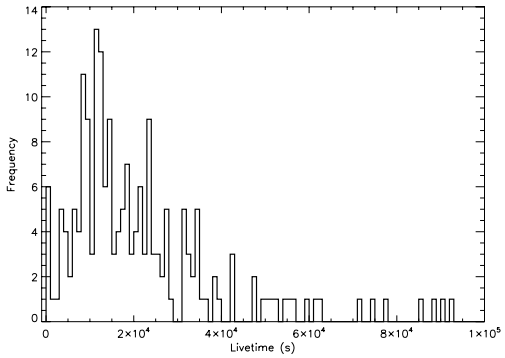

(a) MOS1 livetime histogram after cleaning, all observations

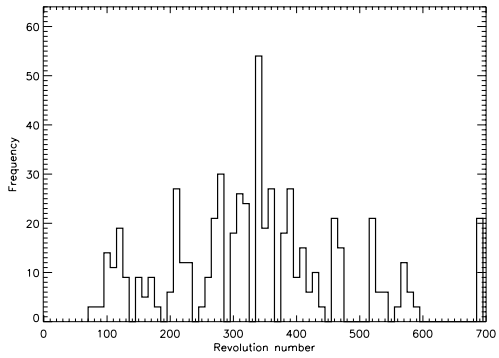

(b) MOS1 revolution number of observation histogram, all observations

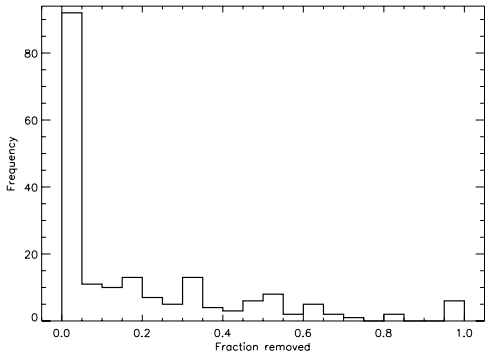

(c) MOS1 fraction of time removed, all observations

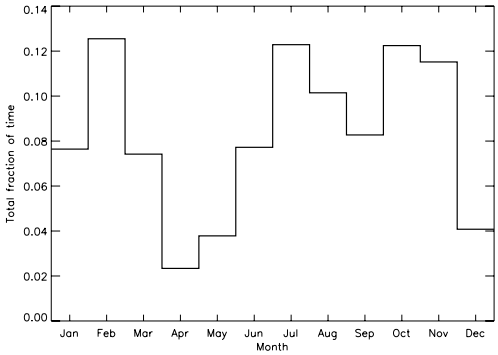

(d) MOS1 fraction of time removed per month, all observations

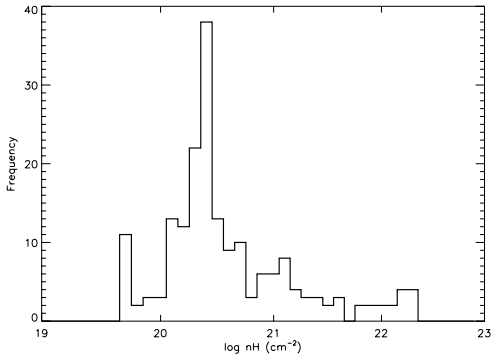

(e) MOS1 histogram of galactic column density values, all observations

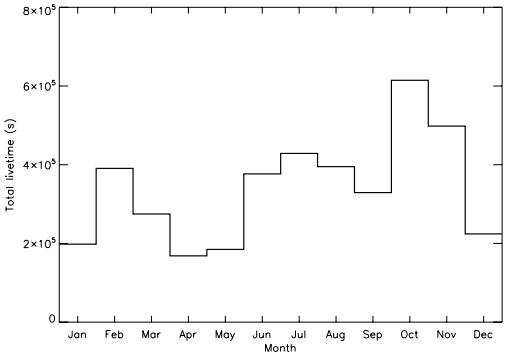

(f) MOS1 livetime per month after cleaning, all observations

Fig. 3. Properties of all the files used to construct the MOS1 blank sky event files; **a)** histogram of livetimes, **b)** histogram of revolution numbers, **c)** fraction of time removed during cleaning, **d)** fraction of time removed per month, **e)** histogram of nH values in the direction of pointing for an observation and **f)** total livetime after cleaning per month.

Figure 4 displays histograms of the fluxes of the sources removed during the cleaning procedure, for each instrument-filter-mode combination. The wide range in observation times used here has led to the low flux edges being rather shallow, i.e. no particular single flux limits exist above which sources have been removed. For a general user, this could lead to some data extracted from the BG event files as being not entirely appropriate – there possibly being slightly too little of too much emission from low-flux sources within the extracted BG data. Future plans for this project (see Sect. 6) include the addition of software able to select BG events files from the full BG dataset of observations, based on the component observation's exposure time. This can lead to BG files with tighter, steeper source flux limit cut-offs, perhaps more appropriate to a user's own single dataset.

3.3. Production of the final files

After the procedure described above was completed for each of the 189 observations, the individual files were reviewed to ensure that no bright sources remained, relevant event files for each instrument-filter-mode combination were merged together to form the final sets (Table 2). Each merged file was subjected to a call to *attcalc* to set the right ascension, declination and position angle to (0, 0, 0). In these final files one will find

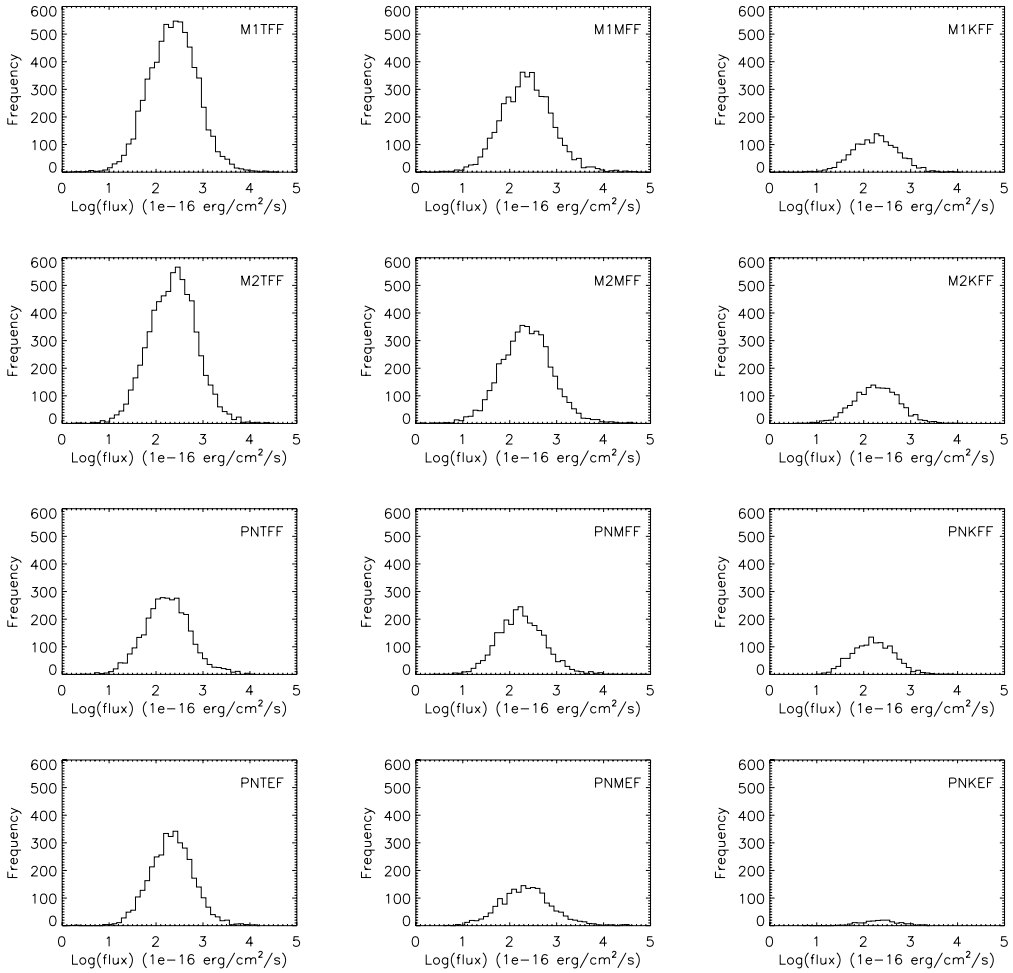

Fig. 4. Flux histograms of the removed sources for each of the instrument-filter-mode combinations data sets, where M1 = MOS1, M2 = MOS2, F = full-frame mode, E = full-frame-extended mode, T = thin filter, M = medium filter and K = thick filter. The y-axis represents the number of sources removed from the data sets for a particular flux.

the primary header, events extension, exposure extensions and GTI extensions. There are 12 exposure and 12 GTI extensions for PN and 7 of both types for each MOS. Keywords that are applicable to only individual observations, such as *DATE_OBS* and *EXPIDSTR* were removed from each file extension. The keywords for *LIVETIME*, *LIVETI0n*, *ONTIME*, and *ONTIME0n*, where n is the number of the CCD, were recalculated and added to the headers of the final file as appropriate. All keywords that are mandatory for OGIP FITS (OGIP_93_003) standards were assured to be present and adjusted. For example the keyword *REVOLUT* was set to 0000, *OBS_ID* was set to 0000000000 and *EXP_ID* was set to 0000000000000.

For both unfilled and refilled PN event files, in the full-frame mode and either the medium or thin filter, it was found that the resultant final file exceeded the size limits for use with the XMM-SAS. It was necessary, therefore to split these files so that they could be usable, and a decision was made to split them based on location on the sky of the events. The files roughly split into hemispheres centred about the galactic centre and the galactic anti-centre as a variation between these two locations is seen in spectral shape, as described in Sect. 4. We here used the addition of the right ascension and declination (RA and Dec) columns added to the component event files in the individual observation processing, which then later appear in the final event files.

For both the unfilled or refilled event lists, this has resulted in the production of 14 final background event files. For each event file there is a corresponding non-vignetted and vignetted exposure map. Therefore there are 84 files in total (42 for either unfilled or refilled procedures).

Table 2 summarises the resulting background event files, detailing the number of component observations used and the overall exposure time.

These final event files offer several improvements over previous blank sky background event files. The ghosting procedure is an addition to the previous work and we have taken advantage of the new 2XMMp reprocessing products and improved general knowledge of the BG to improve the cleaning of each file. These files are found at: `http://xmm.esac.esa.int/external/xmm_sw_cal/background/blank_sky.shtml`. The site includes a description of the naming convention of these files. Images created from the final filled event files can be seen in Fig. 5.

4. Properties of the blank sky event files

Some basic analysis was performed on the blank sky event files. The following features of these data sets should be taken into account when using the files.

Table 2. Summary of the cleaned and filtered observations used in the production of the EPIC background files, separated into the different combinations of instrument, instrument mode and filter used. LIVETIME is the livetime keyword value for the central CCD i.e. corrected for periods of high-background and dead-time. For the PN full-frame mode with the medium or thin filter, the files have been split between the two hemispheres based on the galactic centre and galactic anti-centre individual event pointings.

Instrument	Mode	Filter	Location if applicable	Number of observations	LIVETIME (s)
MOS1	Full-Frame	Thin		113	2 194 330
MOS1	Full-Frame	Medium		65	1 583 390
MOS1	Full-Frame	Thick		12	305 700
MOS2	Full-Frame	Thin		112	2 087 800
MOS2	Full-Frame	Medium		67	1 679 900
MOS2	Full-Frame	Thick		13	343 773
PN	Full-Frame	Thin	total	42	993 370
PN	Full-Frame	Thin	anti-centre	21	536 349
PN	Full-Frame	Thin	centre	21	457 021
PN	Full-Frame	Medium	total	33	1 078 113
PN	Full-Frame	Medium	anti-centre	12	574 272
PN	Full-Frame	Medium	centre	21	503 841
PN	Full-Frame	Thick		10	237 458
PN	Full-Frame-Extended	Thin		62	825 204
PN	Full-Frame-Extended	Medium		30	461 575
PN	Full-Frame-Extended	Thick		3	58 664

4.1. Variations in spectral shape with count rate

Spectra were produced selecting the time intervals for low, medium and high count rates, using good time intervals between 10 keV and 12 keV. Spectra were taken within a circle of radius 8.3′ between 0.3 keV and 8 keV. Using MOS1, thin-filter, full-frame mode as an example, low count rate intervals were defined as those with a count rate less than 48 ct s^{-1}, medium intervals were those with a count rate of between 48 ct s^{-1} and less than 75 ct s^{-1} and those of a high count rates were those with count rates above 75 ct s^{-1}. The intervals were chosen so that the total number of counts in each spectrum was similar to aid comparison. The spectra were plotted using Xspec, using a canned MOS1 response matrix.

Figure 6 shows that the medium and low count rate spectra are comparable, whereas the high count rate spectrum shows enhancement between 0.6 and 8 keV. This effect has been seen before in studies of background removal for cluster analysis (e.g. Temple et al. 2005). Therefore, the user may wish to filter the BG files to an appropriate count rate threshold, based on their own data.

4.2. Variation of out-FOV count rate

For each of the unfilled event lists, the out-of-field-of-view (out-FOV) count rate, essentially the cosmic-ray induced instrumental background, was calculated for both events with pattern 0, and events with patterns ≤12 for MOS and events with patterns ≤4 for PN, using spectra created between the energies of 2.5 keV and 6.0 keV, to avoid the instrumental lines and just show the continuum. The out-FOV count rates representing the quiescent particle (instrumental) background, are given in Table 3.

The count rates for MOS1, MOS2 and PN show an expected increase when looking at the rates from those patterns ≤12, or 4 in the case of PN, compared to those with pattern 0. MOS1 and MOS2 are consistent with each other, whereas PN shows a higher count rate in comparison with the MOS cameras. The PN camera is more sensitive, and the differences in count rates here is indicative of this characteristic.

Differences in count rates are seen between the PN full-frame mode event files (both thin and medium filter), selected on the basis of their sky position – i.e. Galactic centre or Galactic anti-centre – the Galactic centre count rates being somewhat larger. It was initially thought that this difference might be due to the time of year of the individual observations, there being some evidence that summer observations are, on average, more heavily effected by solar flare activity than winter observations. A higher summer-to-winter exposure time ratio for the Galactic centre observations, compared to the Galactic anti-centre observations, could be indicative of relatively worse solar flaring in the Galactic centre observations. These ratios however are not particularly different for the two position-dependent subsets, and thus there is little evidence that this hypothesis is correct. We note though that the numbers of observations in each of the subsets is rather low, and small number statistics and the actual pointings of the individual observations may well be the cause of the observed differences. Indeed, on ignoring outlying observations with high count rates, the ratio between centre and anti-centre is greatly reduced.

4.3. Variation of in-FOV count rates

Similar to the analysis of out-FOV, in-FOV count rates were also taken from spectra between 2.5 keV and 6.0 keV to avoid the instrumental lines, using a circle of 10′, with a pattern selection as before as used for the out-FOV count rates. These values were calculated for the refilled event files to avoid the use of the complicated exposure maps in calculation of the areas used and are also shown in Table 3. For each instrument-filter-mode combination, the in-FOV count rates are higher than those of the out-FOV, as expected as these in-FOV values result from both photon and particle contributions. The MOS cameras are consistent with each other. The PN in-FOV count rates are higher than those of the MOS. The PN in-FOV count rates for those files split into the galactic centre and galactic anti-centre events show the same feature as the out-FOV, namely that the galactic centre has higher count rates than the anti-centre. The factor by which the Galactic Centre count rates are greater than the Galactic anti-centre count rates is larger in-FOV than out-FOV (as expected, given that

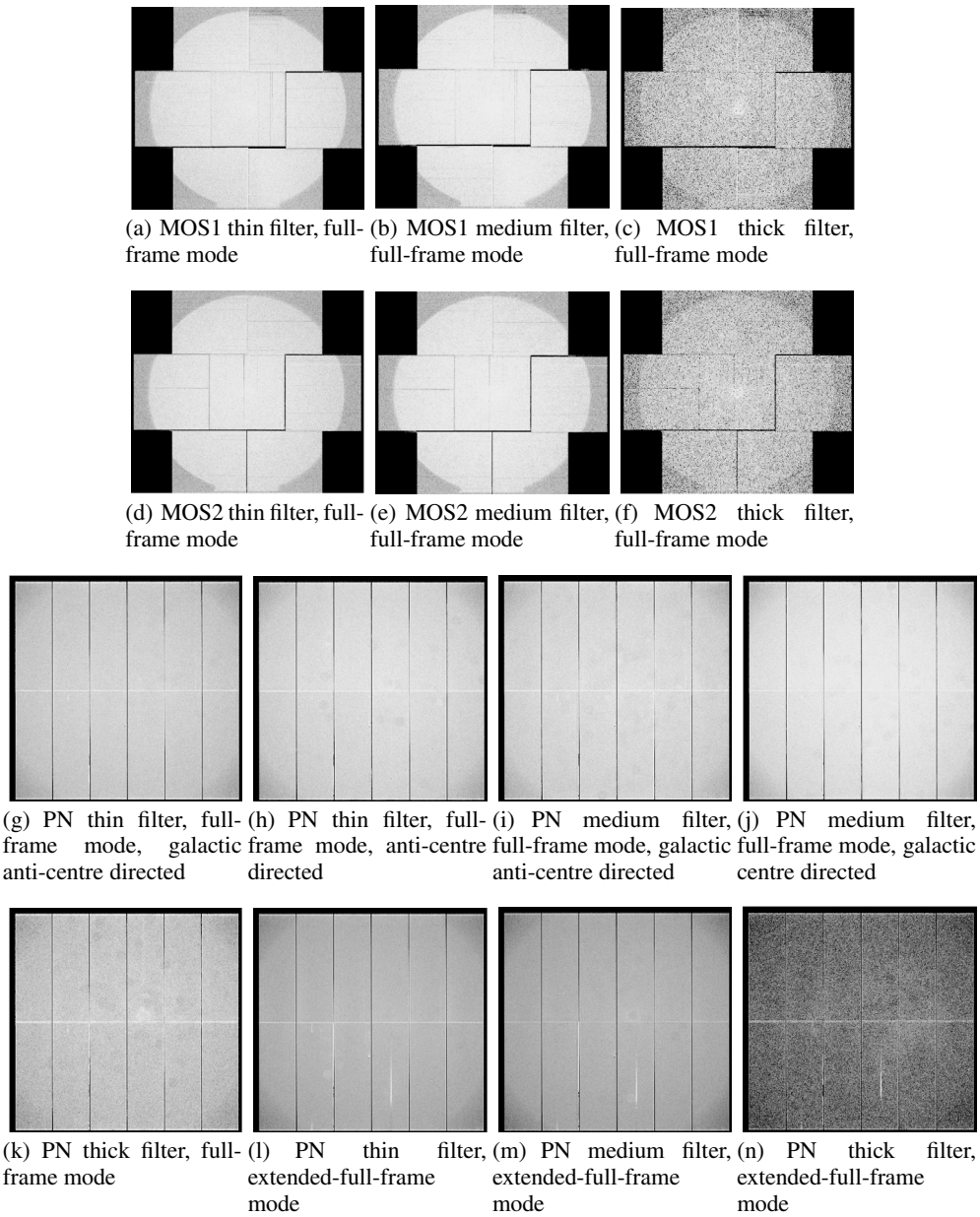

(a) MOS1 thin filter, full-frame mode (b) MOS1 medium filter, full-frame mode (c) MOS1 thick filter, full-frame mode

(d) MOS2 thin filter, full-frame mode (e) MOS2 medium filter, full-frame mode (f) MOS2 thick filter, full-frame mode

(g) PN thin filter, full-frame mode, galactic anti-centre directed (h) PN thin filter, full-frame mode, anti-centre directed (i) PN medium filter, full-frame mode, galactic anti-centre directed (j) PN medium filter, full-frame mode, galactic centre directed

(k) PN thick filter, full-frame mode (l) PN thin filter, extended-full-frame mode (m) PN medium filter, extended-full-frame mode (n) PN thick filter, extended-full-frame mode

Fig. 5. Images of the final unfilled event files for each instrument-filter-mode combination, between 0.3 keV and 12 keV for the PN and from between 0.2 keV and 12 keV for the MOS cameras. The PN event files for full-frame mode, with the medium or thin filters have been split into those events centred about the galactic centre, and those centred about the galactic anti-centre.

photons, soft protons and particles contribute in-FOV, whereas only [mostly] particles contribute out-FOV). As discussed with respect to the out-FOV count rates however, there is no evidence that it is a time-of-year effect that is causing these differences, but it can be explained via statistical fluctuations and the relatively low number of observations used.

An indication of the spectral differences in- and out-FOV, and how these differences can lead to severe problems when trying to subtract the instrumental background, is shown in Fig. 7. Here, MOS1 and pn spectra are shown extracted from the in-FOV region, together with spectra showing the difference between the in-FOV spectrum and an extracted, area-scaled out-FOV spectrum. Strong instrumental BG lines at Al (1.5 keV) and Si (1.7 keV) are seen in the MOS spectrum, together with weaker features at Cr (5.4 keV), Mn (5.8 keV), Fe (6.4 keV) and Au (9.6 keV). The PN spectrum shows a strong instrumental line at Al (1.5 keV) and a strong high-energy line at Cu (8.0 keV), plus weaker high-energy lines at Ni (7.4 keV), Cu (8.6 keV) and Zn (9.0 keV).

The "difference" spectra should, ideally, show what remains once the instrumental BG has been removed, i.e. a smooth photon BG distribution. However this is not the case, and sharp features are seen in the "difference" spectra at the positions of the instrumental lines. This is due to the distribution of the emission from the various fluorescent lines varying across the detectors, as discussed in Sect. 2.1.2. For MOS, there is relative deficit of Al in-FOV compared to out-FOV, hence the "difference" spectrum shows a trough. For Si, the situation is reversed and a peak in the difference spectrum is observed. Similarly Au (2.2 keV) and Fe are relatively enhanced out-FOV. For PN, the Al line is relatively evenly distributed across the detector, and consequently the difference spectrum shows no peak or trough. Ni and Cu however, are very much depleted at the centre of the detector, as discussed

Table 3. Out-FOV and in-FOV count rates for the refilled background event files between 2.5 keV and 6.0 keV. The pattern code gives the patterns used, and can be either equal to 0, ≤12 (MOS) or ≤4 (PN). For the mode/filter combination a code is used, and for some PN files the location dependent of the file is indicated where appropriate [f – full-frame mode, e – full-frame-extended mode, t – thin filter, m – medium filter, k – thick, AC – galactic anti-centre hemisphere, GC – galactic hemisphere].

Instr	Mode/Filt./location if applicable	Pattern code	Out-FOV count rate (2.5−6 keV) (ct/s/arcmin^2)×10^{-4}	In-FOV count rate (2.5−6 keV) (ct/s/arcmin^2)×10^{-4}
M1	ft	0	2.69	5.74
M1	ft	12	4.01	8.17
M1	fm	0	2.80	6.92
M1	fm	12	4.15	9.80
M1	fk	0	2.68	3.52
M1	fk	12	4.02	5.11
M2	ft	0	2.87	5.92
M2	ft	12	4.21	8.92
M2	fm	0	2.93	6.70
M2	fm	12	4.29	9.34
M2	fk	0	2.88	3.48
M2	fk	12	4.22	4.96
PN	et	0	20.4	37.2
PN	et	4	31.2	58.4
PN	em	0	31.3	62.2
PN	em	4	48.1	98.0
PN	ek	0	11.8	17.3
PN	ek	4	17.7	26.8
PN	ft AC	0	25.4	47.7
PN	ft AC	4	39.1	74.9
PN	ft GC	0	34.2	64.1
PN	ft GC	4	52.6	101.0
PN	fm AC	0	27.7	45.3
PN	fm AC	4	42.6	71.1
PN	fm GC	0	39.5	80.1
PN	fm GC	4	61.0	126.5
PN	fk	0	19.0	31.3
PN	fk	4	28.9	49.0

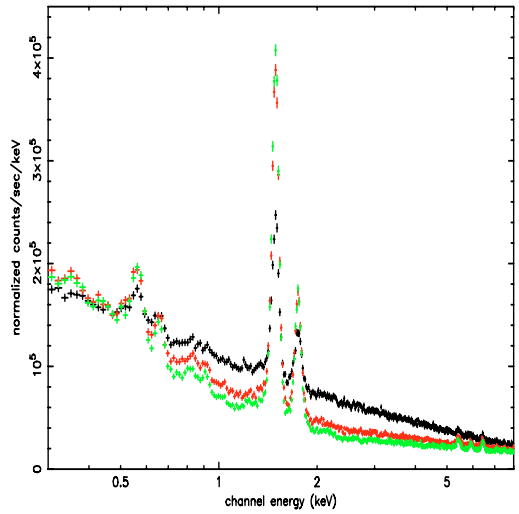

Fig. 6. Spectra plotted based on differences in count rate between 0.3 keV and 8 keV, for MOS1, in full-frame mode using the thin filter. Black shows the highest count rate, red is classed as the medium count rate spectrum, and green the lowest count rate spectrum.

in Sect. 2.1.2, and strong troughs are observed in the difference spectrum.

4.4. Variation in BG with location on sky

Background events from regions of the sky have been selected from four coordinate centres using the script SelectRADec (see Sect. 5): the galactic centre, galactic anti-centre, the south galactic pole and the north galactic pole. Spectra were then produced for each region and plotted in Xspec using a canned response matrix, for example for MOS1 thin filter, full-frame mode as shown in Fig. 8.

Note that the galactic centre shows a higher count rate at between approximately 0.3 keV to 3 keV due to increased soft X-ray emission in the galactic plane and centre.

5. Using the background files

Several useful scripts that can be used with the background event files described in this paper, are found at the BGWG web page. The scripts are described below.

5.1. Script: skycast

This script is used to cast an XMM-Newton EPIC background dataset (or indeed any EPIC event dataset) onto the sky, at the position given by an input template event dataset (e.g. the event file for which one is interested in producing a background). This is useful as the user is more likely to be working in sky coordinates than instrument coordinates.

5.2. Script: selectRADec

This script can be used to select events from a certain area of the sky, specifying a right ascension and declination (J2000), and the maximum distance from this position one is prepared to

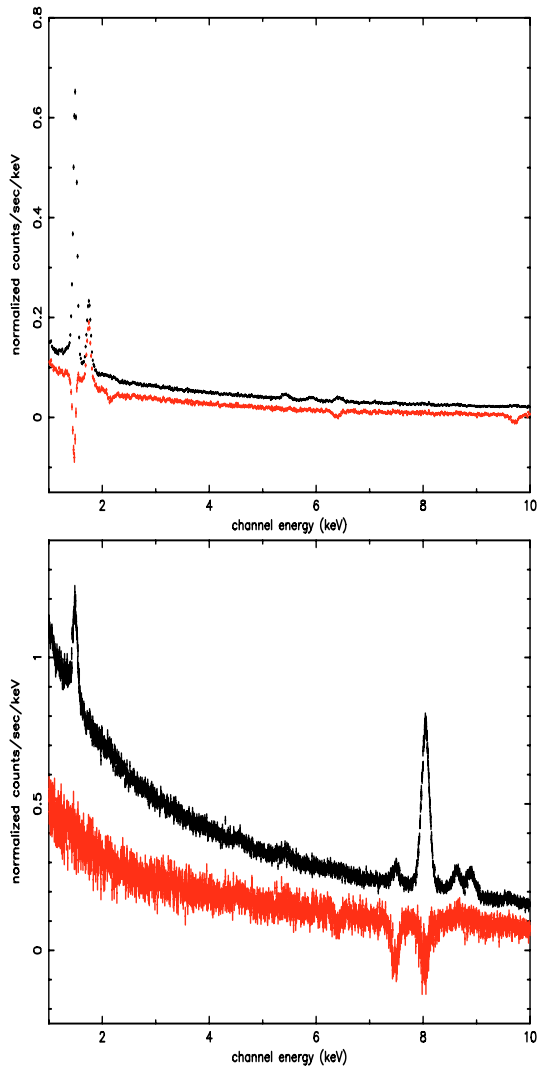

Fig. 7. MOS1 (*top*) and PN (*bottom*) (1.0−10 keV) spectra extracted from the full-frame, thin filter BG event files. The upper spectrum in each panel is extracted from the in-FOV region, while the lower spectrum shows the difference between the in-FOV spectrum and an extracted out-FOV spectrum, scaled to account for the difference in areas. Line features in the "difference" spectra indicate the differences in distribution of fluorescent line emission across the detectors, as explained in the text.

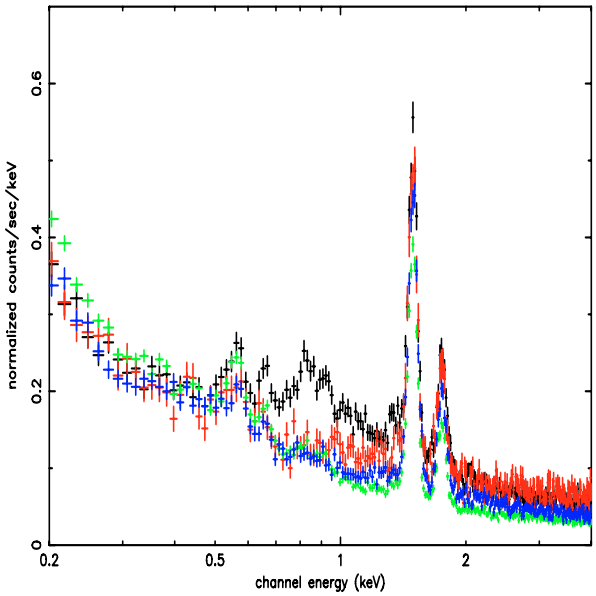

Fig. 8. MOS1 background spectra based on events taken from different sky locations; centred on the galactic centre(black) and anti-centre(red), north(green) and south(blue) galactic poles.

consider. A final event file and exposure map is produced. This may be useful to a user whose is concerned about the dependence of the background with location, as shown in Fig. 8.

5.3. Script: BGrebin

This script is used to rebin and re-project the provided exposure maps onto the sky to the spatial scale and sky position of a user-input image. This is useful when wanting to work in sky coordinates and to a different spatial scale than the 4″ scale used in the production of the exposure maps.

5.4. Using the background files: reliability

In this final subsection on the use of the BG files, we have attempted to provide a gauge of the reliability of the Blank Sky files. To achieve this, and to mirror how these files might be used by the community, we have performed a typical BG analysis that a general user might perform, but on separate *subsets* of the same blank sky event files, and compared the results obtained, i.e. employing a "cross-validation"-like technique. For each analysis, two large time-separated sub-event files were extracted from a particular BG event file, each covering 40−50% of the original exposure time. These two event files were then screened (further) for times of medium-high soft proton flares, as a user would wish to do (the event files having been earlier screened for times of high soft proton flares – see Sect. 3). For each flare-filtered sub-event file, a "source" spectrum was extracted from a 6′ radius circular in-FOV central region of the instrument. A "background" spectrum was also extracted from the out-FOV "corners" of the detector. Here then, the "source" spectrum should contain (predominantly) both photon and particle components of the EPIC BG, whereas the "background" spectrum should contain just the particle component of the EPIC background. Correct analysis and subtraction of one from the other should yield just the extragalactic photon X-ray background.

For the MOS cameras, the out-FOV regions of the detectors are quite large, and hence reasonable instrumental BG statistics can be obtained from these areas (in actuality, we used the MOS out-FOV regions as defined in de Luca & Molendi 2004). For the pn however, the situation is much worse, as the out-FOV regions are very much smaller and close to the noise of the pn readout. The very limited statistics obtained from the pn out-FOV regions make instrumental BG subtraction very problematic. Furthermore, for the pn, the response varies along each CCD due to charge transfer inefficiency effects, making any determination of a linear response with position and radial vignetting a very complicated problem (e.g. Lumb et al. 2002). The recent addition of long-exposure stacks of closed filter full-FOV pn data (dominated by the instrumental BG) to the official ESA web pages (`http://xmm.esac.esa.int/external/xmm_sw_cal/background/index.shtml`. will help in the future to allow a much better determination and subtraction of the

Table 4. Results of spectral fitting to the two subsections of the MOS thin filter, full-frame mode background files, fitted using a wabs×power-law model (see text).

Instr	Subsection	Photon index	Normalisation ($\times 10^{-5}$)
M1	1	1.37 ± 0.15	7.64 ± 1.50
M1	2	1.45 ± 0.15	10.5 ± 1.90
M2	1	1.42 ± 0.07	12.2 ± 1.17
M2	2	1.50 ± 0.19	9.62 ± 2.30

in-FOV instrumental BG component. This is beyond the scope of the present paper however, and we have here concentrated on the MOS data.

The analysis using the large, MOS, thin filter, full-frame BG event files is described here. Once the spectra were formed, as above, appropriate RMF response matrices and ARF auxiliary files were created using XMM-Newton SAS 7.0 and the source spectral channels were binned together to give a minimum of 20 counts per bin. Spectral fitting was performed using Xspec, incorporating a photo-electric absorption times power-law (*wabs*×power-law) model. The hydrogen column density of the absorption component was fixed in each case to the exposure-weighted average of the hydrogen column densities of the component observations (see Sect. 3.2). The power-law spectral index and normalization were allowed to go free. Fitting was performed in the energy range 2.5−6.0 keV, i.e. concentrating on the line-free continuum area of the spectrum. The spectral analysis results are summarized in Table 4. Tabulated, both for MOS1 and MOS2, are the best-fitting power-law spectral index and normalization for each "half" of the original full-size thin filter, full-frame BG event files. Errors are 1σ for one interesting parameter. As can be seen, the fitted indices and normalizations for the two halves are consistent with one another, both for MOS1 and for MOS2. Furthermore, the values obtained for MOS1 are consistent with the values obtained for MOS2. And finally, the actual values of power-law index obtained are consistent with the generally accepted value for the power-law index of the true extragalactic X-ray background (≈1.42; e.g. Lumb et al. 2002). This analysis therefore, indicates that the BG event files presented here are consistent (both with each other and with other external measures of the X-ray BG) and reliable (both between files and internally within individual files).

6. Conclusions and future developments

We have described in detail the components that make up the XMM-Newton EPIC background and why a good understanding of this background is important. We have explained the steps behind the production of blank sky event lists that are available for the general user via the XMM-Newton EPIC background working group website, and are useful for background analysis. We have presented several interesting features of these files including variations in spectral shape with count rate and variations in count rate between out-FOV and in-FOV areas. Finally we have presented software that can be used with the blank sky event files and associated exposure maps, also available via the background working group web pages.

It is hoped that in the near future more 2XMM datasets will become available that fulfil the criteria previously described for the background sets. These will then be filtered as appropriate and merged with the existing datasets. We also hope to improve the ghosting procedure as described in Sect. 3.1 to incorporate the inclusion of bad pixels and columns, and to provide a means to select background events based on their component observation exposure time, as described in Sect. 3.2. A tool to select sections of the event files as based on count rates may become available in the near future, to accompany the tools already available.

Further releases of modified datasets will be announced via the URL: `http://xmm.esac.esa.int/external/xmm_sw_cal/background/index.shtml`.

Acknowledgements. We would like to acknowledge the work of, and thank, all other members and colleagues of the EPIC background working group: M. Ehle, M. Freyberg, M. Kirsch, K. Kuntz, A. Leccardi, S. Molendi, W. Pietsch and S. Snowden. We thank and acknowledge the anonymous referee for helpful and useful comments that have improved this paper.

References

De Luca, A., & Molendi, S. 2004, A&A, 419, 837
Freyberg, M., Briel, U. G., Dennerl, K., et al. 2004, Proc. SPIE, 5165, 112
Jansen, F., Lumb, D., Altieri, B., et al. 2001, A&A, 365, L1
Kuntz, K. D., & Snowden, S. L., in prep.
Lumb, D., Warwick, R. S., Page, M., & de Luca, A. 2002, A&A, 389, 93
Nevalainen, J., Markevitch, M., & de Lumb, D. 2005, ApJ, 629, 172
Pradas, J., & Kerp, J. 2005, A&A, 443, 721
Read, A., & Ponman, T. 2003, A&A, 409, 395
Snowden, S. L., Collier, M. R., & Kuntz, K. D. 2004, ApJ, 610, 1182
Strüder, L., Briel, U., Dennerl, K, et al. 2001, A&A, 365, L18
Temple, R. F., Pratt, G. W., Ponman, T. J., et al. 2005, in The X-ray Universe, SP-604, 753
Turner, M. J. L., Abbey, A., Arnaud, M., et al. 2001, A&A, 365, L27